

A Novel On-Board Electrochemical Impedance Spectroscopy System for Real-Time Battery Impedance Estimation

Markos Koseoglou^{ID}, Student Member, IEEE, Evangelos Tsioumas^{ID}, Student Member, IEEE, Dimitrios Papagiannis, Student Member, IEEE, Nikolaos Jabbour^{ID}, and Christos Mademlis^{ID}, Senior Member, IEEE

Abstract—This article proposes a real-time electrochemical impedance spectroscopy (EIS) technique that can provide high accurate estimation of the impedance of each lithium-ion (Li-ion) cell of a battery (BT) stack, even for less than $m\Omega$. Thus, the suggested EIS technique can be used in high demanding applications, such as nearly zero-energy buildings, microgrids, and electric vehicles. This is attained because a smooth cell excitation current is utilized that is provided by the proper control of the gate-source of each cell's parallel-connected MOSFET and thus, effective harmonic analysis can be accomplished. Since the circuit topology of the EIS is implemented without requiring expensive electronic equipment, it is affordable to be applied in the BT system of any application. The proposed EIS system can cooperate with a BT cell equalization (BCE) system that utilizes the same MOSFET control scheme to provide the excitation current. Thus, a combined EIS–BCE system is developed that can be used to improve the performance of a Li-ion BT management system. The accuracy of the EIS technique and its high performance by operating within a combined EIS–BCE system are experimentally validated.

Index Terms—Battery cell equalization (BCE), battery (BT) management system, electrochemical impedance spectroscopy (EIS), energy storage system, microgrid and electric vehicle.

I. INTRODUCTION

IT IS well known that the electrochemical energy storage is increasingly emerged as the key technology which can play a crucial role in the improvement of the energy sustainability, in several sectors of the everyday life [1]. Especially, the wide-spread penetration of renewable energy and distributed generation in power networks, as well as, the increasing electric mobility have become significant fields of interest for the use of the energy storage systems [2].

The lithium-ion (Li-ion) battery (BT) is a key technology for the future energy storage systems [3] due to the competitive

Manuscript received July 24, 2020; revised November 4, 2020 and January 7, 2021; accepted February 25, 2021. Date of publication March 3, 2021; date of current version June 1, 2021. This work was supported by the European Union and Greek National Funds through the Operational Program Competitiveness, Entrepreneurship and Innovation, under the call RESEARCH–CREATE–INNOVATE under Project T1EDK-00399. Recommended for publication by Associate Editor K.-B. Lee. (*Corresponding author: Nikolaos Jabbour*)

The authors are with the Department of Electrical Energy, School of Electrical and Computer Engineering, Aristotle University of Thessaloniki, Thessaloniki 54 124, Greece (e-mail: markkose@ece.auth.gr; etsioumas@ece.auth.gr; dipapagi@auth.gr; njabbour@auth.gr; mademlis@auth.gr).

Color versions of one or more figures in this article are available at <https://doi.org/10.1109/TPEL.2021.3063506>.

Digital Object Identifier 10.1109/TPEL.2021.3063506

advantages against the other BT types, such as the high energy density, the high charge/discharge current capability, and the low self-discharge rate [4]. Although, the Li-ion BTs could be considered as a promising solution, they have several drawbacks that should be considered during the design of an energy storage system, i.e., limited cycle and calendar life, higher cost, sensitivity in extreme temperature conditions, and safety issues. Moreover, the Li-ion BTs performance is highly sensitive to overvoltage/undervoltage and overcurrent. Therefore, in order to protect the performance and the lifespan of a Li-ion BT cell, it should operate within the voltage, temperature, and current rate limits, as that are defined by the manufacturer.

A common characteristic of the Li-ion BTs is the low operating voltage, and thus, several cells should be connected in series to meet the voltage requirements. This may cause imbalance problems in a BT stack that are mainly owed to the different internal characteristics of the cells, such as the coulombic efficiency, the capacity, and the self-discharge rate [5]. Moreover, internal resistance growth and capacity fade along with potential imbalance issues may result to significant reduction of the power and energy capability of a BT system [6].

The above mentioned can be avoided by properly controlling the cells of a Li-ion BT stack in order to reduce the imbalance effects and keep each cell operation within safety and acceptable limits of the voltage, current, and temperature [7]. Thus, several BT cell equalization (BCE) methods have been proposed in the technical literature that can be classified as energy dissipative and nondissipative [8]. The dissipative cell balancing methods are simpler and low cost; however, the equalization electric energy is wasted in heat. In the nondissipative methods, the equalization energy is transferred among the other cells and thus, they are more efficient [9]. However, they are more expensive and complicated in the implementation and thus, more susceptible to faults that may result to reduction of the BT system reliability [10].

For the proper operation of a BT system, it is highly important the accurate knowledge of the operating parameters of each BT cell, in real-time basis, such as the state of charge (SoC), state of health (SoH), and state of function (available charging and discharging power, SoF) [11]. Since the aforementioned parameters cannot be directly measured, they are usually estimated by utilizing the BT model that is however highly influenced by the ageing level [12]. Therefore, several techniques have been

proposed to accurately estimate the BT model parameters, so as, the model is updated with respect to the actual operating conditions [13]. However, due to the increase in the cost and complexity, these techniques are rarely embedded in a BT system [14].

It is well known that the impedance of a Li-ion BT can provide important information for the electrochemical condition within the cell that can be utilized for the accurate evaluation of the BT state. Therefore, an easily implemented and cost-effective estimation method of each cell impedance can be a useful tool for a high performance BT system [15]. One widespread noninvasive estimation method of the Li-ion BT impedance is the electrochemical impedance spectroscopy (EIS) [16], that has been adopted by several laboratory instruments for offline measurements of the cell impedance for a wide frequency range [17] and has also been utilized to estimate the BT model parameters [18].

The EIS technique can be categorized in *single frequency*, where the individual frequencies are measured sequentially and *broadband*, that utilizes multiple simultaneous sinusoidal excitations [19]. Although the broadband methods are faster than the single frequency, they need larger time to settle to a steady-state response that may diminish the above advantage. On the other hand, the benefits of the single-frequency techniques are the higher accuracy and effectiveness in the EIS performance, since the fundamental frequency of each operation cycle is known *a priori*. Therefore, less interference by the noise in the impedance estimation is caused compared to the broadband methods, where advanced computation techniques are needed to reject the noise that may result to the increase of the complexity [20], [21].

It is well known that the frequency spectrum of interest for the BT cell's impedance estimation ranges from a few kHz to several mHz and thus, the EIS can be accomplished with the single-sine technique at an acceptable time duration [22]. Therefore, considering the capabilities of high accuracy and effectiveness, lower complexity and with an acceptable duration for the impedance estimation procedure, the single-frequency technique can be the suitable choice for an EIS system [23]. This is confirmed by the growing interest of the electronic equipment industry that works on the development of ICs to facilitate the real-time single-frequency EIS techniques for Li-ion BTs, such as [24].

Due to the advantages that the EIS technique can provide in the accurate estimation of the Li-ion BT impedance, it attracts a growing research interest by the research community. Thus, the research efforts are toward the development of an EIS system which can accurately and in real time estimate the cells' impedance, that then can be used for the evaluation of several BT operating states, such temperature and online modeling, as well as, various operating parameters, such as SoC, SoH, and SoF have been pointed out in [25]–[28]. However, most of the published online EIS techniques are focused on the estimation of the impedance of the whole BT pack [29]–[41] and consequently, they do not provide information for the individual operating state of each cell that it could effectively contribute to the improvement of the BT system performance. Moreover, they use external power sources for the injection of

the excitation current, such as the motor controller [31] and BT chargers based on several type dc–dc conversion topologies, such as dc–dc boost converter [29] and bidirectional dc–dc converter [30], as well as, ac–dc conversion topologies, such as dual active bridge converter [39] and single-phase two-level full-bridge converter [40]. Consequently, the implementation of the above EIS techniques is directly dependent on the external power sources and consequently, they cannot be embedded in an individually operated BT system.

Although an EIS technique that can real time estimate the impedance of each cell of a BT pack has been proposed in [42], it has been focused on BT cells with relatively high impedance (61.3 mOhms). However, this does not correspond to BT systems for high demanding applications such as nearly zero-energy buildings, microgrids, and electric vehicles, since their impedance is in the range of mOhms so as they are capable to provide the relatively high current which is required by those applications [43]. The limitation to relatively high impedance of the [42] is owed to the implementation of the EIS technique that has been designed for a low excitation current, since a high excitation current that could allow low values of cell's impedance estimation may increase the cost and the volume of the nondissipative dc–dc converter layout and thus, it may become less practical for a real application. Some other attempts for online EIS impedance estimation on the cell level have been conducted in [44], [45]; however, the frequency range is confined with respect to the lower frequencies to 11 Hz, which do not cover the required frequency range for Li-ion cells. The above publications do not give explicit information for the EIS software and they are referred to a relatively high energy capacity BT system utilizing a dc–dc converters' topology with ultracapacitors and switch matrix devices for the implementation of the cell equalization. Consequently, a larger frequency range for the EIS procedure may result to significantly increase of the hardware requirements and complexity.

From the above, it is revealed that there is a need for an improved and effective EIS technique in an integrated scheme of hardware topology and software algorithm that is capable to accurately estimate Li-ion BT cells impedance even for less than mOhm. Moreover, it should be easily implemented and cost-effective, so as, it can be affordable to be embedded in a Li-ion BT system. Therefore, it can be utilized in a wide range of Li-ion BT systems and more important, for high demanding applications, such as nearly zero-energy buildings, microgrids, and electric vehicles. Moreover, the hardware topology should ensure high accuracy in the measurements and the injection of the proper excitation current. Therefore, high performance of the EIS procedure and satisfactory accuracy of the cell impedance estimation can be attained.

The aim of this article is to fulfill all the above requirements and to propose an effective and highly accurate EIS technique that can real time estimate the impedance of Li-ion BT cell over a wide frequency range. The accuracy of the cell impedance estimation is attained through an advanced system of hardware topology and a Fourier analysis based calculation algorithm. Thus, contrarily to the up to now published EIS techniques that use sophisticated switching topologies based on ac–dc and dc–dc

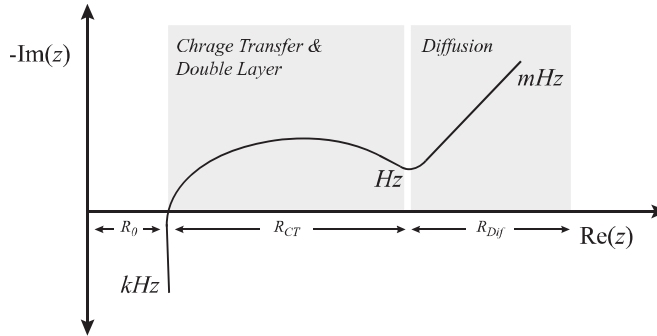


Fig. 1. EIS Nyquist plot representation.

converters in order to inject the variable frequency excitation signal, the proposed EIS system employs a simpler and more reliable topology that is based on using a MOSFET in parallel connection with each BT cell that acts as controllable source to provide the required excitation current. The regulation of the excitation current is attained through the proper control of the gate source of the MOSFET. Therefore, a smooth current profile is provided for accomplishing accurate and effective EIS procedure. Also, the requirements of low complexity, and thus, less vulnerability to faults as well as low cost are met, and thus, the proposed EIS scheme can be applied to any BT system. Moreover, the proposed EIS system can be housed on the BT control electronic board and thus, it can independently operate with respect to the power charger and the BT-powered application. The accuracy of the suggested EIS technique is validated by comparing it with a commercial laboratory instrument, while the high performance is experimentally verified by examining its operation within a combined EIS–BCE system for a Li-ion BT scheme of two series connected cells.

II. UNDERLYING THEORY OF EIS

The EIS is considered as a nondestructive characterization technique that allows the physical interpretation and modeling of the underlying phenomena that takes place inside a Li-ion BT cell [46]. It can be used either in potentiostatic mode, where the voltage is used as excitation signal and the current as measurement signal, or in galvanostatic mode, where the opposite series in the signals is applied [47]. In most commonly used EIS applications, the excitation signal is a sinusoidal reference signal, and the real and the imaginary parts of the BT impedance can be estimated by the measurement signals [48]. The variation of the impedance of a BT cell with respect to the frequency, as resulted by the EIS technique, is more commonly represented by Nyquist and bode plots.

A typical Nyquist plot obtained by the EIS technique is illustrated in Fig. 1. The real part of the impedance is attributed to the ohmic character of the Li-ion BT cell, while the imaginary part is referred to the capacitive and inductive character. The plot can be divided into three regions with respect to the working frequency [49]–[51]. Specifically, the high-frequency region on the left (in the range of kHz) is mainly attributed to the ionic resistance of the electrolyte, the ohmic resistance of the metal

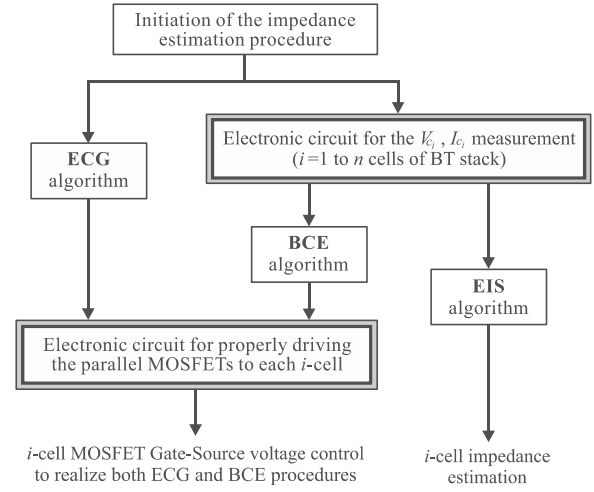


Fig. 2. Structure overview of the proposed BT cell impedance estimation scheme based on the EIS technique.

parts of the electrodes and the inductive behavior of the cell, whose role is more important as the frequency increases. The mid frequency region (kHz–Hz), where the semicircle occurs, represents the charge transfer and the double layer phenomenon which occurs at the area between the electrolyte and the electrodes. Depending on the chemistry and the degradation level of a BT, a second semicircle may occur between the high-frequency and the mid-frequency regions, that is attributed to the solid electrolyte interphase layer, which is created on the negative graphite electrode. Finally, the low-frequency region (Hz–mHz) represents the mass transport effects, which are mainly affected by the diffusion phenomena in the active materials inside the electrodes.

III. OVERVIEW OF THE PROPOSED EIS METHODOLOGY

The structure overview of the proposed BT cell impedance estimation scheme based on the EIS technique and combined with the BCE system is illustrated in Fig. 2. When the impedance estimation procedure is initiated, the excitation current generation (ECG) algorithm instructs an electronic circuit to provide the correct excitation current profile to each BT cell, as that is needed for the impedance calculations through the EIS algorithm. This electronic circuit comprises a MOSFET in parallel connection with the corresponding BT cell and a drive unit to regulate the operation of the MOSFET through the proper control of its gate-source voltage. The excitation current that is commanded by the ECG is a sinusoidal signal with controllable amplitude and frequency that can be injected, either in conjunction with the BCE system or only for the EIS operation.

The EIS algorithm measures the voltage and current of each cell, V_{ci} and I_{ci} , respectively, and provides the impedance estimation that can be used for the calculation of several BT operation parameters. Note that, the BCE algorithm runs with a certain sampling ratio, while the combined system of ECG and EIS algorithms operate asynchronously and when the cell impedance estimation is required.

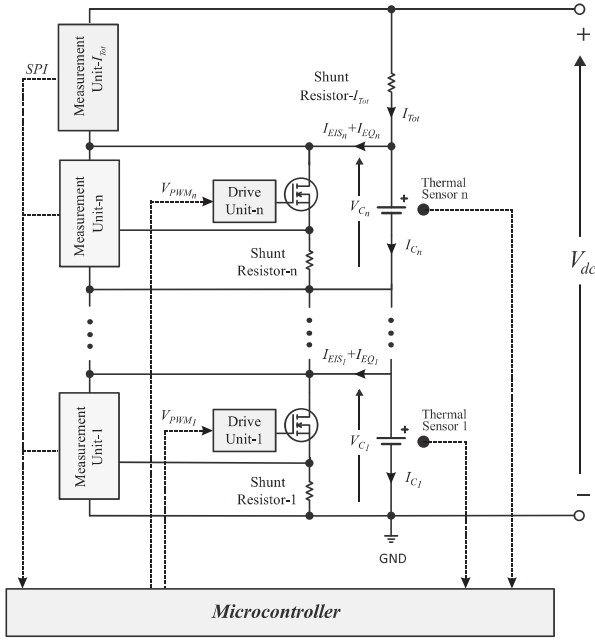


Fig. 3. Structure overview of the hardware topology for the implementation of the impedance estimation procedure based on the EIS technique.

The proposed EIS system can accurately estimate the BT cell's impedance irrespective of the level of the load current, since the frequency of the excitation current is a priori known and also, smooth equalization current is provided by properly regulating the gate source of the parallel connect MOSFET to each BT cell. Moreover, since the proposed EIS procedure is applied during the charging of the BT system of which the performance is properly controllable, high dynamic performance is not observed.

IV. STRUCTURE OF THE PROPOSED CONTROL SCHEME

The structure overview of the hardware topology of the proposed BT cell impedance estimation technique is shown in Fig. 3. It comprises the measurement and the drive units, the MOSFETs that are in parallel connection with the corresponding cells, and the appropriate temperature sensors for each i -cell. The voltage, current, and temperature measurements are provided to the microcontroller through the serial peripheral interphase (SPI) protocol and are used by both the EIS and BCE systems. Each drive unit regulates the gate-source voltage of the corresponding MOSFET through the PWM signal that is provided by the microcontroller for realizing both the EIS and BCE procedures.

A. BT Cell Measurement Unit

The schematic layout of a measurement unit that is used to measure the voltage and the current of each cell and the whole BT stack is illustrated in Fig. 4. The four-terminal Kelvin measurement topology is used for both the voltage and the current measurements. A gain programmable instrumentation amplifier is used to measure the differential voltage across each BT cell, in order to eliminate any interferences with respect to the ground potential that could be introduced in the case of a single-ended

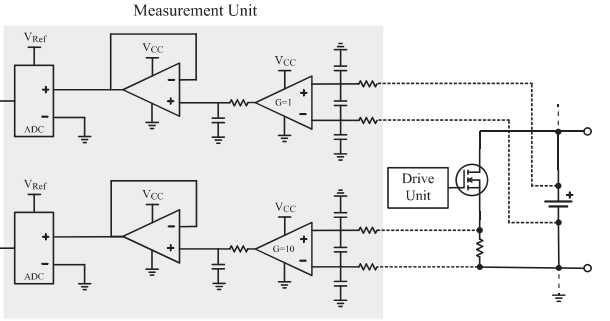


Fig. 4. Schematic layout of the measurement unit that is utilized in the implementation scheme of the EIS-based impedance estimation procedure.

measurement. The cell voltage and current measurements are buffered via an operational amplifier (Op-Amp), and they are provided to the ECG-EIS and BCE systems through the analog to digital converters (ADCs), utilizing the SPI protocol.

The gain for the cell voltage measurement has been set to 1 V/V. The gain for the shunt voltage measurement has been set to 10 V/V, while the exact gain for the current measurement depends on the proper selection of the shunt resistor. Finally, an external voltage reference is used for the ADCs in order to improve the accuracy of the measurements.

B. BT Cell MOSFET Drive Unit

To produce the excitation and equalization currents for the EIS and BCE systems, respectively, the methodology of [52] has been adopted. Specifically, the excitation and equalization currents are provided by properly regulating the operation of each MOSFET that is parallel connected to the corresponding BT cell. Thus, each MOSFET operates at the saturation region and acts as a controllable source by properly regulating the gate-source voltage through the respective controllers. Therefore, unlike the highly pulsating current that would be applied if the MOSFET was in parallel connection with a fixed resistance which would be in series with the BT cell, a smooth current profile is provided with the above proposed configuration that can contribute to the effective harmonic analysis of the EIS and consequently, high accuracy of the cell's impedance estimation is accomplished.

Note that, when the BT system is online, the excitation current of the EIS is superimposed on the equalization current of the BCE, and consequently, a unique current with the proper profile is provided by the MOSFET. Whereas, when the BT system is offline, only the excitation current is supplied to the corresponding cell. Thus, one current with the correct profile is provided by one power source (the parallel connected MOSFET at each BT cell) that is controlled by the combined EIS-BCE procedure. Since the excitation current of the EIS is superimposed on the equalization current of the BCE, they do not influence each other and the two procedures can independently operate. Moreover, since a common power source is utilized, less hardware and lower complexity are attained. Contrarily, if a decoupled hardware topology of two power sources had been used (i.e., two dc-dc converters), the hardware requirements and

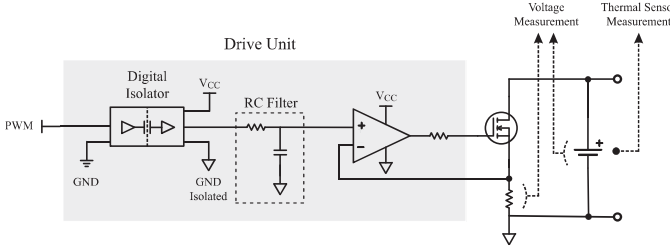


Fig. 5. Schematic layout of the mosfet drive unit that is utilized in the implementation scheme of the EIS-based impedance estimation procedure.

the control complexity would be increased without providing any advantageous features to the performance of the EIS and BCE.

The schematic layout of the MOSFET drive unit for both the EIS and BCE procedures is illustrated in Fig. 5. As can be seen, the topology is based on the current control of the MOSFET via the feedback measurement from the shunt resistor. The input PWM signal is isolated via the digital isolator and it is converted to an analog signal by the resistor–capacitor (RC) filter in order to drive the noninverting input of the Op-Amp. The MOSFET current is regulated by properly controlling the voltage drop across the feedback shunt resistor based on a closed-loop logic control technique and therefore, it is not affected by the delay that the RC filter may introduce, nor it is based on the ideal curve of the MOSFET. Since the voltage across the inputs of the Op-Amp increases as the number of series connected BTs increases, an isolation interface is needed in order to properly control the current at each MOSFET. Specifically, high speed isolators have been adopted, in order to isolate each drive unit and with adequately large bandwidth, in order to get the maximum response on the high-frequency range of the EIS excitation current.

Since each MOSFET provides smooth current profile for both the EIS and BCE procedures by operating in the saturation region through the proper regulation of the gate-source voltage, and thus, it does not operate with high switching frequency, it seems unlikely to fail during the normal operation. However, since the BT safety is extremely important, each MOSFET circuit is protected by a fuse. Note that, a specialized fault tolerance system or a backup system to replace any potential problematic MOSFETs will considerably increase the cost, the complexity, and the size of the system and consequently, it is avoided.

V. REAL-TIME EIS-BASED ESTIMATION ALGORITHM

The flowchart that describes the proposed impedance estimation algorithm is illustrated in Fig. 6. It needs the measurements of the voltage and current of each i -cell, V_{c_i} and I_{c_i} , respectively, of the n cells of the BT stack. The ECG algorithm is activated by the enable command and it produces the proper reference excitation current I_{EIS_i} for each i -cell, which consists of sequential series of k -order frequency sinusoidal signals with controllable amplitude. The I_{EIS_i} current can be either superimposed on the cell equalization current I_{EQ_i} of the BCE (when the BT

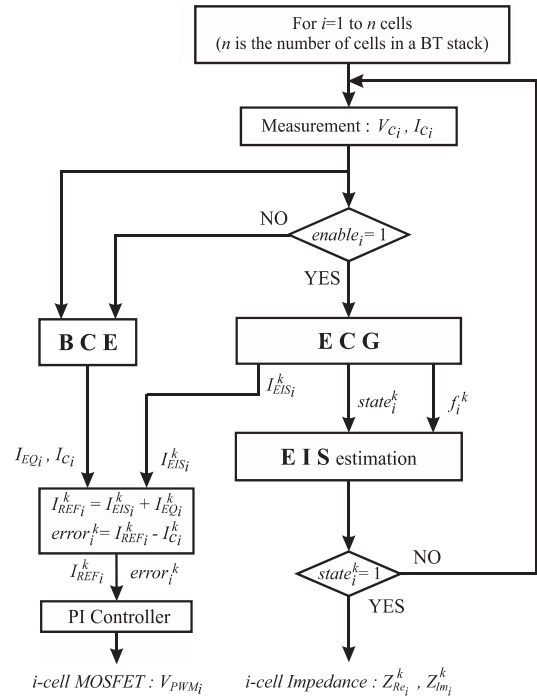


Fig. 6. Flowchart of the proposed real-time EIS estimation algorithm.

system is online) or it is solely supplied to the corresponding i -cell (when the BT system is offline). Thus, for each k -order frequency $I_{EIS_i}^k$, the resulting reference excitation current $I_{REF_i}^k = I_{EIS_i}^k + I_{EQ_i}$ is compared with the actual current I_{c_i} of the i -cell, that is obtained by the measurement unit. Then, the $error_i^k = I_{REF_i}^k - I_{c_i}^k$ is driven to a digital proportional-integral (PI) controller and the output is a PWM signal that controls the gate-source voltage of the corresponding MOSFET and consequently, the BT current I_{c_i} . Instead of the PI controller, a fuzzy-logic controller or simply a proportional control unit could be used to drive the gate source of the MOSFET. However, the PI controller exhibits better performance due to its integral control term.

The ECG, apart from the I_{EIS_i} generation, is also responsible to regulate the operation of the EIS estimation procedure of any i -cell, through the $state_i^k$, and also to inform the EIS algorithm for the frequency f_i^k of the excitation current. The output of the EIS estimation procedure is the real and the imaginary part of the impedance Z_i^k of each i -cell of the Li-ion BT stack, per k -order frequency f_i^k .

A. ECG Algorithm

The ECG algorithm determines the proper excitation current for the effective performance of the EIS procedure and the satisfactory estimation of the Li-ion BT cells impedance. The frequency range, the number of the signal periods, and the impedance estimation points per decade of the excitation current play a crucial role for the proper performance of the EIS [53], [54]. Specifically, the frequency range should be properly chosen, so as, both the diffusion phenomenon at low frequencies

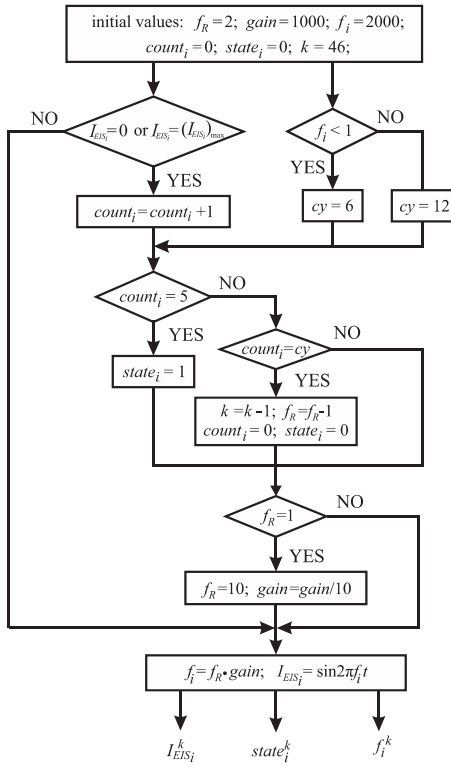


Fig. 7. Flowchart of the ECG algorithm.

and the zero cross ohmic resistance at high frequencies are satisfactorily considered. The number of the signal periods per k -order frequency should ensure both short EIS procedure duration and satisfactory time margin for the proper estimation of the i -cell impedance. Also, an acceptable number of impedance estimation points per decade should be provided, so as, satisfactory information for the impedance variation throughout the whole frequency range are acquired. The above parameters should be properly determined before the EIS procedure is initiated by considering the specific requirements of the Li-ion BT system application. For the examined case, the frequency range is selected from 2 kHz to 20 mHz, since frequencies outside of this range do not provide important information for the impedance of Li-ion BTs and also, it is selected that the cell impedance is estimated at nine points per decade. Thus, the total points for the five logarithmic decades of the frequency range 1 kHz to 20 mHz is 45 and adding one point that corresponds to the frequency of 2 kHz, we have 46 impedance estimation points for the chosen frequency range 2 kHz to 20 mHz.

The flow chart of the ECG algorithm is shown in Fig. 7. It runs from the higher to lower frequencies with logarithmic variation of the step frequencies. The operation margins for each k -order frequency are delimited by the zero crossing and maximum value points of the excitation signal. A schematic representation of the excitation current profile is illustrated in Fig. 8.

The initial values for the variables in the Fig. 7 are determined based on the previous analysis and the fact that the algorithm runs from the high to the minimum frequency limits. Specifically, the initial value of the f_R variable corresponds to the running point

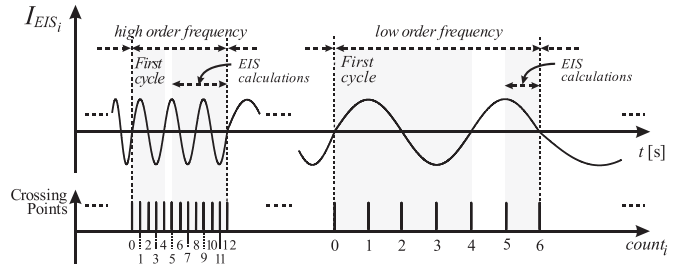


Fig. 8. Schematic representation of the cell excitation current for the EIS procedure.

per decade (initially 2, for the starting frequency of 2 kHz), the gain variable determines the decade of the frequency points (initially 1000 for the 1–10 kHz decade), and the f_i variable corresponds to the running frequency (starting frequency 2 kHz). The counters $count_i$ and $state_i$ are initiated by the zero value, while the cy variable is the limit for the counter $count_i$ and it takes values 6 and 12. Finally, the estimation point variable k that is used in the tables which store the results of the EIS procedure starts with the value 46 that corresponds to the maximum number of the estimation points.

As mentioned above, the frequency changes logarithmically with nine frequency orders per decade, while adapted number of cycles are used per order. Specifically, three cycles are applied at higher frequencies (greater than 1 Hz), while it is reduced to 1.5 cycles for the lower frequencies (less than 1 Hz). This is allowed because a smooth cell current (sum of excitation and equalization current) is provided due to the proposed MOSFET control topology and thus, there is no need for high settle time to reach the steady state. Therefore, a quarter of a cycle is sufficient for the low frequencies to get satisfactory measurements and to provide accurate impedance estimation. The impedance measurements acquisition is enabled at the end of the first $1^{1/4}$ cycle of the excitation current, since additional to the first cycle, a quarter of cycle is needed due to the delay of the voltage signal with respect to the current which is owed to the capacitive nature of the BT cell. For the higher frequencies, since the period per cycle has been reduced and considering the microcontroller frequency, a larger time interval is needed (at least three cycles) for accomplishing both, satisfactory settling to a steady-state condition and accurate impedance estimation.

The above setting in the number of cycles, with respect to the frequency order, shortens the duration of the EIS procedure and also ensures satisfactory accuracy in the impedance estimation. Thus, for the frequency range from 2 kHz to 20 mHz, the total impedance estimation points are 46, and the total duration of the EIS procedure is 5.4 min.

The zero-crossing and maximum value points of the excitation current are counted by the variable $state_i^k$ (for the i -cell and k -order excitation current). As can be seen in the flow chart of Fig. 7, when the variable $count_i$ is equal to 5, it means that $1^{1/4}$ periods of the k -order frequency excitation current have been completed and thus, the variable $state_i$ becomes 1 and the EIS estimation procedure results are received. When the $count_i$ is equal to 6 (for the low frequencies $f_i < 1$ Hz), it means that 1.5

cycles of the k -order frequency have been completed, while, if it is equal to 12 (for the higher frequencies, $f_i \geq 1$ Hz) it means that three cycles have been completed. Thus, for both cases, the variable state_{*i*} gets the value 0 and the frequency of the excitation current is reduced by one order ($k-1$). It is also examined if the nine frequency orders, per decade, of the excitation current have been completed, and if this occurs, the frequency moves to the next decade by decreasing the parameter gain to gain/10.

B. EIS Procedure for the Cell Impedance Estimation

For each k -order frequency, the results of the EIS procedure are acquired when the variable state_{*i*}^{*k*} gets the value 1 (Fig. 6). Since the BT cell current is created by the sum of the excitation and the equalization currents, the Fourier analysis is utilized to obtain the fundamental voltage and current for each k -order frequency. Thus, the measured voltage and current V_{c_i} and I_{c_i} , respectively, are multiplied by cosine and sine signals and then, the Fourier components are calculated by the numerical integrations of the following:

$$a_{V_{c_i}}^k = \frac{2}{T^k} \int_{t_h}^{T^k + t_h} V_{c_i}(t) \cos(2\pi f_i^k) dt \quad (1)$$

$$b_{V_{c_i}}^k = \frac{2}{T^k} \int_{t_h}^{T^k + t_h} V_{c_i}(t) \sin(2\pi f_i^k) dt \quad (2)$$

$$a_{I_{c_i}}^k = \frac{2}{T^k} \int_{t_h}^{T^k + t_h} I_{c_i}(t) \cos(2\pi f_i^k) dt \quad (3)$$

$$b_{I_{c_i}}^k = \frac{2}{T^k} \int_{t_h}^{T^k + t_h} I_{c_i}(t) \sin(2\pi f_i^k) dt \quad (4)$$

where T^k is the period of the k -order frequency excitation current and t_h is the time instant that the measurements are obtained. Therefore, the amplitude and the phase of the impedance are determined, respectively, by

$$|Z_i^k| = \sqrt{\left(a_{V_{c_i}}^k\right)^2 + \left(b_{V_{c_i}}^k\right)^2} \quad (5)$$

$$\varphi_{Z_i^k} = \arctan\left(\frac{b_{V_{c_i}}^k}{a_{V_{c_i}}^k}\right) - \arctan\left(\frac{b_{I_{c_i}}^k}{a_{I_{c_i}}^k}\right) \quad (6)$$

and thus, the real and the imaginary parts of the impedance are

$$\text{Re}(Z_i^k) = |Z_i^k| \cos(\varphi_{Z_i^k}) \quad (7)$$

$$\text{Im}(Z_i^k) = |Z_i^k| \sin(\varphi_{Z_i^k}). \quad (8)$$

As aforementioned, during the quarter of a cycle, for the low frequencies and $1^{3/4}$ cycles for the high frequencies, the EIS algorithm obtains the *i*-cell voltage and current measurements and determines the real and the imaginary parts of the impedance for the k -order frequency.

VI. EXPERIMENTAL RESULTS

The theoretical considerations of this article have been experimentally verified on a high-power Li-ion BT cell (Melasta LPB042126H) with nominal capacity, voltage, and discharge current of 7.4 Ah, 3.7 V, and 10 C, respectively. The control software is realized on the microcontroller TMS320F28379D, which communicates with the measurement and drive units via the SPI protocol and PWM signals, respectively. The running frequency of both the EIS procedure and the PI controller is 40 kHz, while the frequency of the excitation current ranges from 2 kHz to 20 mHz. Thus, both the EIS procedure and the PI controller are faster than the excitation current (e.g., the EIS procedure and PI controller are 20 times faster for the maximum excitation current of 2 kHz and this ratio increases as the excitation current frequency reduces) and also, they are faster than the monitoring and equalization processes of the BCE system, for which the sampling ratio is 1 kHz.

The measurement unit comprises the LTC2368 ADC, the LT6657 with reference voltage 5 V and the LT6370 instrumentation amplifier. The gain for the cell voltage measurement has been set to 1 V/V, while the gain for the 100 mΩ shunt current resistor has been set to 1 A/V. The signals are digitized through the 5 V, 24-bit ADC, which results to a sense resolution of 0.3 μV and 3 μA for the voltage and current, respectively. The shunt resistor of 100 mOhm handles the dc equalization current of 1 A plus the ac current of the EIS of 1 A (peak value). Thus, the maximum thermal power at the shunt resistor is 0.29 W, which is considered acceptable compared to its thermal rating that is 5 W. In case that lower heat generation on the shunt resistor is required, the ohmic value of the shunt resistor should be reduced.

The synchronization of the current and voltage measurements is critical to attain high accuracy at the BT cell's impedance estimation, especially at the imaginary part of the impedance, which is mainly determined by the phase difference between the voltage and the current measurements. This is accomplished by independently programing the conversion process of the ADC and the sampling process of the microcontroller. Specifically, the conversion process of the voltage and current measurements are simultaneously triggered via a common digital signal, and the measurements are provided to the microcontroller through a daisy chain configuration with sampling rate 200 Ksps (5 μs). Therefore, the microcontroller receives the synchronized measurements by the ADCs.

The frequency of the PWM signal provided by the microcontroller is 100 kHz and the cut-off frequency of the RC low-pass filter is adjusted to 7.96 kHz (the R and C components are 200 Ω and 0.1 μF, respectively). Therefore, the low-pass filter can act as a digital to analog converter for providing a smooth signal to the Op-Amp, while at the same time, the cut-off frequency is sufficiently larger than the excitation frequency. Furthermore, the Op-Amps that are used both in the drive and the measurement units have a bandwidth at the range of MHz, which is much faster than the maximum frequency of the excitation signals.

The accuracy of the proposed EIS technique has been experimentally validated by comparing the estimated impedance of the tested BT cells with a commercial laboratory instrument

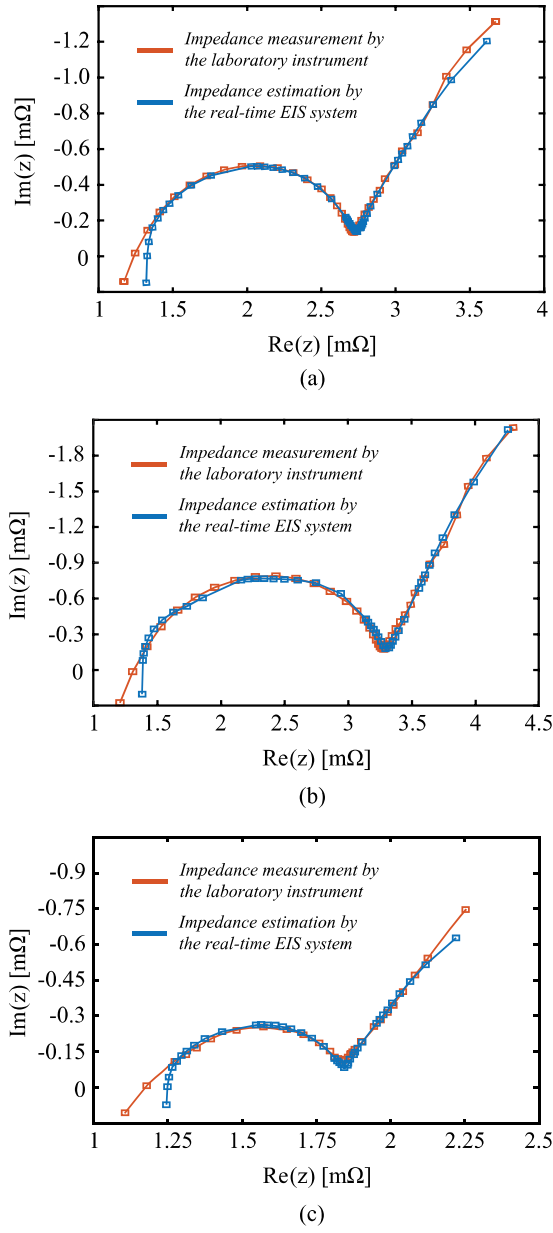


Fig. 9. Comparison of the proposed prototype with a commercial laboratory instrument: (a) 50% SoC and 25°C operating temperature, (b) 10% SoC and 25°C operating temperature, and (c) 50% SoC and 35°C operating temperature.

(Metrohm Autolab ECI10M with a 10 A booster and a four-wire measurement setup). As explained in Section IV, the proposed algorithm is logarithmically performed with nine impedance measurements per decade for a frequency range from 2 kHz to 20 mHz, that results to 46 measurement points, per each impedance estimation procedure. In order to have a common comparison basis, the same measurement setup is used for the laboratory instrument and also, the same BT cells at the same operating conditions (voltage, temperature, and current) are used.

In Fig. 9, the BT cell's impedance estimation obtained by the proposed EIS system is compared with the impedance estimation obtained by the laboratory instrument, which can be considered

as the reference estimation. Three cases are examined for the same BT cell, for various SoC and temperature conditions. Specifically, Fig. 9(a) illustrates the impedance estimation for 50% SoC and 25°C operating temperature, Fig. 9(b) for 10% SoC and 25°C operating temperature, and Fig. 9(c) for 50% SoC and 35°C operating temperature.

The measurements with the proposed EIS system and the laboratory instrument for each of the above three sets have been done within some minutes and with at least three days between each set of measurements. Thus, common comparison basis with respect to relaxation time is ensured, i.e., conduction of the experiments for the same operating conditions at almost the same time period and enough relaxation interval between the three sets of measurements [55], [56].

As can be seen in the inverted Nyquist plots of Fig. 9, the impedance estimated by the proposed EIS system is in good agreement with the reference measurements for all the examined cases and only some small discrepancies occur at the very high and very low frequencies. The small discrepancies that occur at the very high frequencies are owed to the fact that the number of the sampling points per signal period is reduced, as the frequency of the excitation current is increased. Also, since these discrepancies occur at the frequency range 2 kHz–800 Hz that corresponds to a small operating time interval of 0.011 s, they could not be attributed to the BT cell polarization or any change in the operating characteristics. Thus, if higher accuracy is required, the sampling frequency should be increased. Note that, in the experimental system, the sampling ratio at the higher frequency of 2 kHz is 20 measurement points per signal period, since the running frequency of the EIS procedure is 40 kHz, and the number of the sampling points increases as the examined frequency reduces. Thus, the cell's impedance estimation accuracy is improved at the lower frequencies. However, small discrepancies are observed at the very low frequencies, which are significantly smaller than that at the high frequencies. These discrepancies can be attributed to the different impact that may have the changes in the BT cell operating parameters, which are observed during the relatively large duration of the low frequency measurements, on the EIS estimation of the laboratory instrument methodology against the proposed technique.

The impedance measurement accuracy is also quantified by analyzing the rms error for the real and imaginary parts. The rms error for the real part is given by

$$\varepsilon_{\text{Re}} = \sqrt{\frac{1}{N} \sum_{j=1}^N [\text{Re}_1(f_j) - \text{Re}_2(f_j)]^2} \quad (9)$$

where the subscript 1 indicates the data obtained by the proposed EIS system, the subscript 2 indicates the data obtained by the laboratory reference instrument, and f_j is the frequency at each measurement point j , for the $N = 46$ points. Similarly, the rms error in the imaginary part is given by

$$\varepsilon_{\text{Im}} = \sqrt{\frac{1}{N} \sum_{j=1}^N [\text{Im}_1(f_j) - \text{Im}_2(f_j)]^2} \quad (10)$$

From (9) and (10), the rms errors for the real and imaginary parts of the impedance estimation by the proposed EIS procedure with respect to the reference estimation from the laboratory

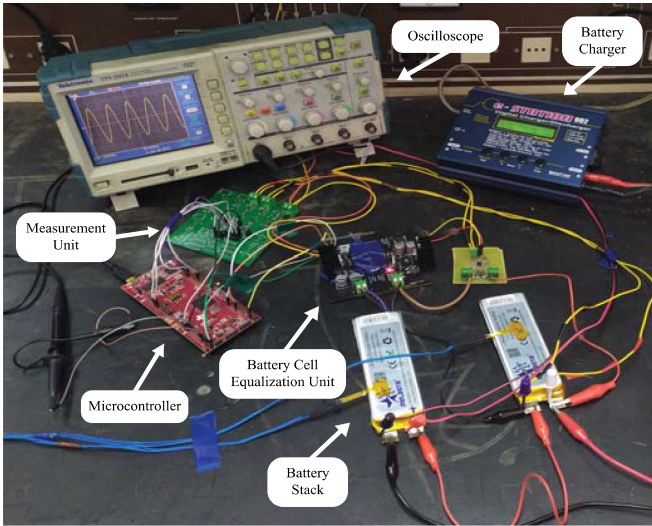


Fig. 10. Layout of the experimental system with the proposed combined EIS–BCE system.

instrument are 0.012 and 0.017 mΩ, respectively, which can be considered negligible compared to the actual impedance value.

It should be noted that the four-terminal Kelvin measurement technique is applied for the voltage measurements, in order to eliminate the influence of the contact resistance effect. Specifically, two separate wires are used for the voltage sensing that are directly connected to the BT cell terminals and thus, the comparison of the cell impedance estimation between the proposed EIS system and the laboratory instrument can be considered accurate [57]. However, in some BT system applications, the mounting of the cells may introduce contact resistance even in the case of four-terminal Kelvin measurements. In that cases, the contact resistance should be considered, and an identification technique should be used, such as that proposed in [58].

The effective cooperation of the proposed real-time EIS system with the BCE technique has been experimentally validated by utilizing the prototype EIS system with two series connected BT cells. The layout of the experimental system is illustrated in Fig. 10. The two BT cells have different internal performance parameters, specifically, the Cell₁ is new, while the Cell₂ has been cycled many times and it is considered degraded. The above layout of two series connected BT cells is indicative and only for the purpose of the current experiments, since the proposed EIS–BCE technique can effectively estimate the BT impedance regardless of the number of series and parallel connected cells. The excitation current should be selected based on the typical rule of the ac perturbation of ~10 mV [56].

The proposed EIS technique is used both for the evaluation of the BT ageing, when the system is disconnected from the charger, and in cooperation with the cell equalization algorithm, during the charging procedure. Thus, it is examined the performance of the proposed EIS technique for both offline and real-time operation during charging. Specifically, the BT ageing evaluation is performed when the BT system is disconnected and operates independently from the charging procedure. During the real-time operation, the algorithm of [52] is adopted for the

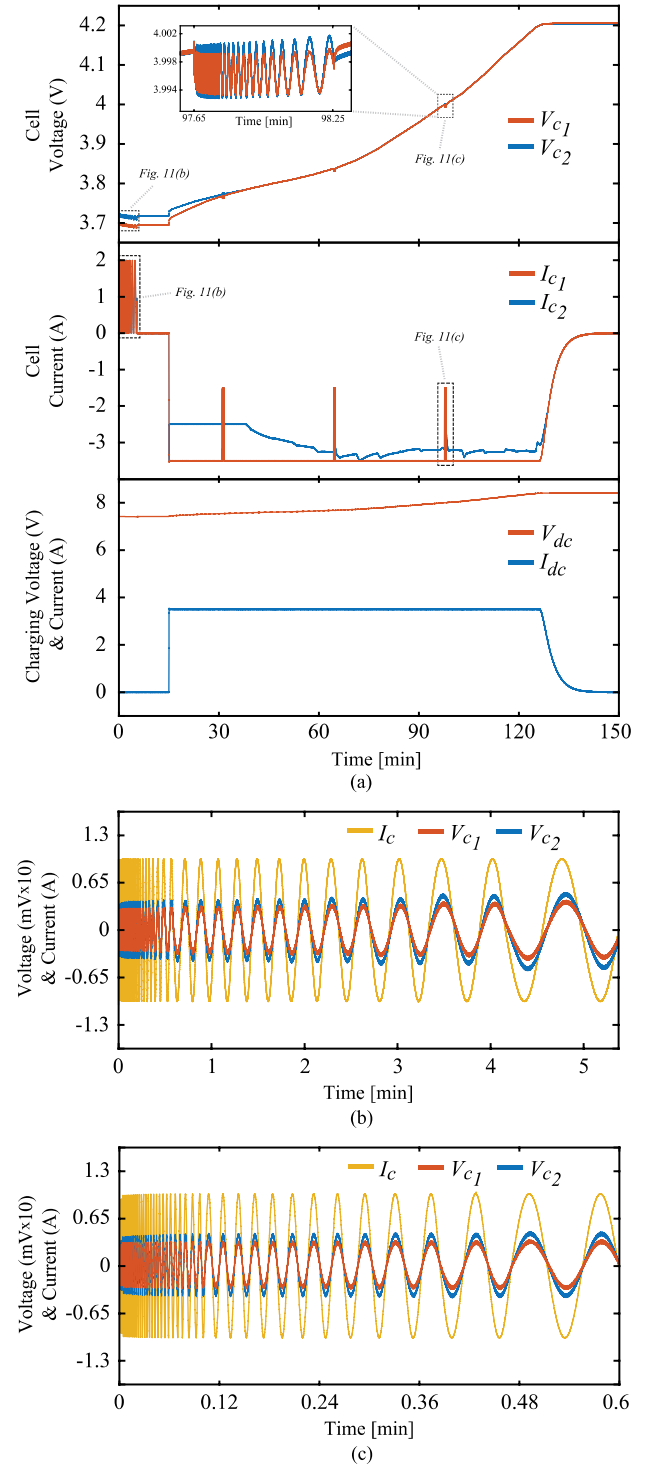


Fig. 11. Experimental results of the performance of the proposed combined EIS–BCE system for real-time operation: (a) whole procedure, (b) first EIS procedure of duration 5.4 min, and (c) fourth EIS procedure of duration 0.6 min.

balancing of the series-connected BT cells and the proposed EIS procedure is realized at specific time points that are initiated by trigger signals provided by the BCE.

The performance of the combined EIS–BCE system for real-time operation is shown in Fig. 11. As can be seen, the EIS procedure is initiated when the BT system is in an idle mode

with approximately 20% SoC and after 30 min of rest from the last discharge. It lasts 5.4 min for the whole frequency range of 2 kHz–20 mHz and it is realized by applying an ac current of amplitude 1 A, which is considered a satisfactory trade-off between sufficient signal-to-noise ratio and minimal change in system linearity for the examined BT, based on the typical rule of the ac perturbation of ~ 10 mV [56]. Then, the system remains in an idle situation for an interval of approximately 10 min. This time interval has been decided arbitrarily, just to separate the EIS for the BT ageing evaluation from the real-time EIS procedure during the BT charging. After the 10 min idle period, the charging procedure is started and the activation of the EIS is regulated by the BCE at specific time intervals. During the charging of the BT system, the duration of each EIS procedure has been reduced to 0.6 min, which is much shorter than the EIS at the BT charging evaluation, since the frequency range has been decreased to 2 kHz–0.2 Hz. The confinement of the frequency range and consequently the shortening in the EIS duration is allowed because during the real-time operation, the information for the zero-crossing and the charge transfer resistances is enough for the proper BT cell balancing. Thus, the low-frequency diffusion region can be omitted to significantly reduce the EIS implementation time. Note that the required energy is 0.037 Wh for the 0.6 min procedure and 0.333 Wh for the 5.4 min procedure, which correspond to the 0.13% and 1.2% of the nominal BT capacity, respectively. In case that the proposed EIS technique operates during the charging mode, the above driving energy is provided by the BT charger. The EIS technique can also operate when the BT is in discharging mode; however, since in this case the driving energy is provided by the BT, it should be evaluated if and how often the EIS procedure should be conducted.

The current and the voltage of the BT cells during the EIS, for the initial EIS procedure of duration 5.4 min and the fourth EIS procedure of duration 0.6 min, are shown in Fig. 11(b) and (c), respectively. The BT cells impedance estimations of the above real-time EIS procedures are illustrated, in Nyquist plots, in Fig. 12(a) and (b), respectively. As can be observed, the EIS satisfactorily cooperates with the BCE (Fig. 11) and it can effectively give the impedance estimations (Fig. 12). Note also that, the EIS can effectively estimate that the BT Cell₂ is significantly degraded, since both the high- and the mid-frequency impedances are greater than the respective impedances of the new BT Cell₁. Furthermore, the local maximum point occurs at significantly decreased frequency (at 100 Hz for the new Cell₁ compared to 40 Hz for the aged Cell₂). This means that, apart from the impedance increase, the time constant of the cell has increased and thus, it is confirmed the degradation of the Cell₂.

Since the proposed EIS technique is a real-time procedure, the accuracy of the impedance estimation is not affected by the polarization effect that it is observed when the BT is rest for a short period. However, the impacts of the polarization and any other electrochemical effects such as the temperature and the SoC variations, that may occur during the use of the BT, affect the BT internal characteristics and thus, they are reflected on the cell's impedance. Therefore, the real-time BT impedance

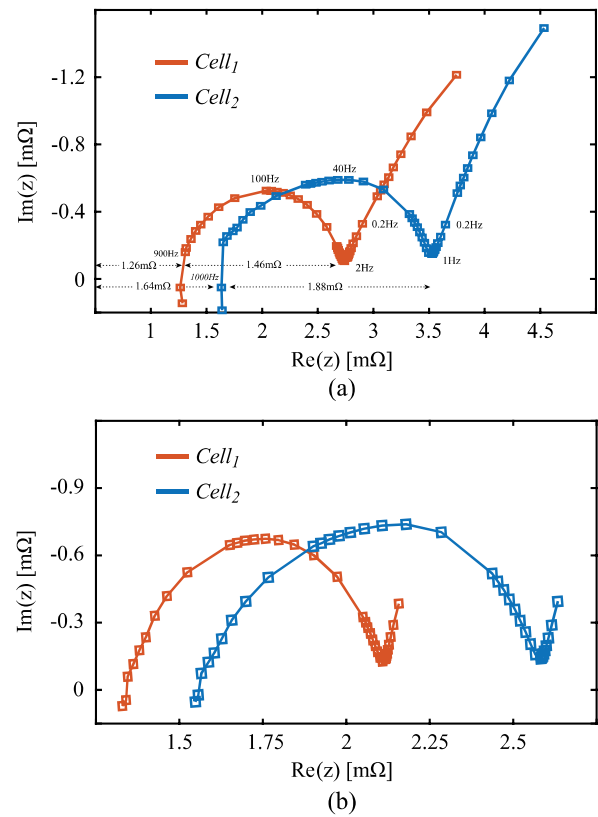


Fig. 12. Nyquist plots of the BT cells impedance obtained by (a) initial real-time EIS procedure of duration 5.4 mins and (b) fourth real-time EIS procedure of duration 0.6 min.

estimation through the proposed EIS method considers the aforementioned effects and thus, the current BT operating condition can be effectively evaluated.

It should be noted that, although the BCE method of [52] has been adopted in this article, the proposed real-time EIS system can be utilized by any other BCE technique, such as the [59], where an hierarchical SoC balancing controller is used along with a multi-input single-output power converter for each series BT module and back-to-back MOSFETs for each parallel BT of the module. In the case of [59], the multi-input single-output power converter can be replaced by the proposed on-board EIS system and along with the back-to-back MOSFETs can be used for the impedance measurement of each BT cell in the series-parallel configuration of the system.

VII. CONCLUSION

In this article, a real-time EIS technique combined with a BCE system has been proposed that can accurately estimate the BT cell impedance. The proper excitation current for the performance of the EIS technique is provided by a MOSFET that is in parallel connection with each BT cell and acts as a controllable current source, for both cell impedance estimation and cell equalization. Therefore, a smooth current profile is provided that ensures accurate and effective EIS procedure. The circuit topology of the EIS is implemented without requiring

expensive electronic equipment, and therefore it is affordable to be applied in the BT system of any application. Additionally, due to the effective harmonic analysis that the smooth cell excitation current can provide, the proposed EIS technique can accurately estimate the BT cell impedance even at the range of mOhms and thus, it can be used in high demanding applications. The accuracy of the proposed EIS technique has been validated by comparing it with a commercial laboratory instrument. Also, the effectiveness and the practicality in the implementation of the proposed combined EIS–BCE system have been experimentally validated with two series connected BT cells, for demonstrating the use of the system in a real-time application.

ACKNOWLEDGMENT

The authors would like to thank Ms. A. Touni and Prof. S. Sotiropoulos from the Chemistry Department of Aristotle University of Thessaloniki, for providing the EIS laboratory instrument for the measurements.

REFERENCES

- [1] J. B. Goodenough and K.-S. Park, "The Li-ion rechargeable battery: A perspective," *J. Amer. Chem. Soc.*, vol. 135, no. 4, pp. 1167–1176, 2013.
- [2] N. Hatzigyriou, H. Asano, R. Iravani, and C. Marnay, "Microgrids," *IEEE Power Energy Mag.*, vol. 5, no. 4, pp. 78–94, Jul./Aug. 2007.
- [3] A. Yoshino, "Development of the lithium-ion battery and recent technological trends," *Lithium-Ion Batter.*, pp. 1–20, 2014.
- [4] G. L. Plett, *Battery Management Systems: Battery Modeling*. Boston, MA, USA: Artech House, 2015.
- [5] G. L. Plett, "Extended kalman filtering for battery management systems of lipb-based HEV battery packs: Part 1. Background," *J. Power Sources*, vol. 134, no. 2, pp. 252–261, 2004.
- [6] J. Vetter *et al.*, "Ageing mechanisms in lithium-ion batteries," *J. Power Sources*, vol. 147, no. 1/2, pp. 269–281, 2005.
- [7] G. L. Plett, "Extended kalman filtering for battery management systems of lipb-based HEV battery packs: Part 2. Modeling and identification," *J. Power Sources*, vol. 134, no. 2, pp. 262–276, 2004.
- [8] S. K. Dam and V. John, "A modular fast cell-to-cell battery voltage equalizer," *IEEE Trans. Power Electron.*, vol. 35, no. 9, pp. 9443–9461, Sep. 2020.
- [9] M. Koseoglou, E. Tsionumas, N. Jabbour, and C. Mademlis, "An improved active Li-ion battery equalization scheme for enhancing the performance of a nearly zero energy building and electric vehicle microgrid," in *Proc. IEEE 4th Southern Power Electron. Conf.*, 2018, pp. 1–7.
- [10] D. Andrea, *Battery Management Systems for Large Lithium-Ion Battery Packs*. Boston, MA, USA: Artech House, 2010.
- [11] W. Waag, C. Fleischer, and D. U. Sauer, "Critical review of the methods for monitoring of lithium-ion batteries in electric and hybrid vehicles," *J. Power Sources*, vol. 258, pp. 321–339, 2014.
- [12] K. Li, F. Wei, K. J. Tseng, and B. Soong, "A practical lithium-ion battery model for state of energy and voltage responses prediction incorporating temperature and ageing effects," *IEEE Trans. Ind. Electron.*, vol. 65, no. 8, pp. 6696–6708, Aug. 2018.
- [13] C. Fleischer, W. Waag, H.-M. Heyn, and D. U. Sauer, "On-line adaptive battery impedance parameter and state estimation considering physical principles in reduced order equivalent circuit battery models part 2. Parameter and state estimation," *J. Power Sources*, vol. 262, pp. 457–482, 2014.
- [14] M. Dubarry *et al.*, "Battery energy storage system modeling: A combined comprehensive approach," *J. Energy Storage*, vol. 21, pp. 172–185, 2019.
- [15] C. Fleischer, W. Waag, H.-M. Heyn, and D. U. Sauer, "On-line adaptive battery impedance parameter and state estimation considering physical principles in reduced order equivalent circuit battery models: Part 1. Requirements, critical review of methods and modeling," *J. Power Sources*, vol. 260, pp. 276–291, 2014.
- [16] A. Barai *et al.*, "A comparison of methodologies for the non-invasive characterisation of commercial Li-ion cells," *Prog. Energy Combustion Sci.*, vol. 72, pp. 1–31, 2019.
- [17] W. Waag, S. Käbitz, and D. U. Sauer, "Experimental investigation of the lithium-ion battery impedance characteristic at various conditions and aging states and its influence on the application," *Appl. Energy*, vol. 102, pp. 885–897, 2013.
- [18] L. H. J. Rajmakers *et al.*, "Sensorless battery temperature measurements based on electrochemical impedance spectroscopy," *J. Power Sources*, vol. 247, pp. 539–544, 2014.
- [19] J. Sihvo, D. Stroe, T. Messo, and T. Roinila, "Fast approach for battery impedance identification using pseudo-random sequence signals," *IEEE Trans. Power Electron.*, vol. 35, no. 3, pp. 2548–2557, Mar. 2020.
- [20] S. Gantenbein, M. Weiss, and E. Ivers-Tiffée, "Impedance based time-domain modeling of lithium-ion batteries: Part I," *J. Power Sources*, vol. 379, pp. 317–327, 2018.
- [21] T. N. Güçin and L. Ovacik, "Online impedance measurement of batteries using the cross-correlation technique," *IEEE Trans. Power Electron.*, vol. 35, no. 4, pp. 4365–4375, Apr. 2020.
- [22] B. Bulecks, R. Suresh, and R. Rengaswamy, "Rapid impedance measurement using chirp signals for electrochemical system analysis," *Comp. Chem. Eng.*, vol. 106, pp. 421–436, 2017.
- [23] C. Schaeff, E. Din, and J. T. Stauth, "A hybrid switched-capacitor battery management IC with embedded diagnostics for series-stacked li-ion arrays," *IEEE J. Solid-State Circuits*, vol. 52, no. 12, pp. 3142–3154, Dec. 2017.
- [24] "Panasonic develops battery management technology to measure electrochemical impedance of multi-cell stacked lithium-ion batteries," 2019. [Online]. Available: <https://news.panasonic.com/global/press/data/2019/11/en191114-2/en191114-2.pdf>
- [25] A. A. Hussein and A. A. Fardoun, "An adaptive sensorless measurement technique for internal temperature of li-ion batteries using impedance phase spectroscopy," *IEEE Trans. Ind. Appl.*, vol. 56, no. 3, pp. 3043–3051, May/Jun. 2020.
- [26] J. Sihvo, T. Roinila, and D. Stroe, "Novel fitting algorithm for parametrization of equivalent circuit model of li-ion battery from broadband impedance measurements," *IEEE Trans. Ind. Electron.*, vol. 68, no. 6, pp. 4916–4926, Jun. 2021.
- [27] Z. Xia and J. Abu Qahouq, "State-of-charge balancing of Lithium-ion batteries with state-of-health awareness capability," *IEEE Trans. Ind. Appl.*, vol. 57, no. 1, pp. 673–684, Jan./Feb. 2021.
- [28] O. Theliander, A. Kersten, M. Kuder, W. Han, E. Arfa Grunditz, and T. Thiringer, "Battery modeling and parameter extraction for drive cycle loss evaluation of a modular battery system for vehicles based on a cascaded H-bridge multilevel inverter," *IEEE Trans. Ind. Appl.*, vol. 56, no. 6, pp. 6968–6977, Nov./Dec. 2020.
- [29] E. Sadeghi, M. H. Zand, M. Hamzeh, M. Saif, and S. M. Mahdi Alavi, "Controllable electrochemical impedance spectroscopy: From circuit design to control and data analysis," *IEEE Trans. Power Electron.*, vol. 35, no. 9, pp. 9933–9942, Sep. 2020.
- [30] S. M. R. Islam and S. Park, "Precise online electrochemical impedance spectroscopy strategies for li-ion batteries," *IEEE Trans. Ind. Appl.*, vol. 56, no. 2, pp. 1661–1669, Mar./Apr. 2020.
- [31] D. A. Howey, P. D. Mitcheson, V. Yufit, G. J. Offer, and N. P. Brandon, "Online measurement of battery impedance using motor controller excitation," *IEEE Trans. Veh. Technol.*, vol. 63, no. 6, pp. 2557–2566, Jul. 2014.
- [32] W. Huang and J. A. Abu Qahouq, "An online battery impedance measurement method using DC–DC power converter control," *IEEE Trans. Ind. Electron.*, vol. 61, no. 11, pp. 5987–5995, Nov. 2014.
- [33] M. A. Varnosfaderani and D. Strickland, "A comparison of online electrochemical spectroscopy impedance estimation of batteries," *IEEE Access*, vol. 6, pp. 23668–23677, 2018.
- [34] R. Koch, R. Kuhn, I. Zilberman, and A. Jossen, "Electrochemical impedance spectroscopy for online battery monitoring—Power electronics control," in *Proc. 16th Eur. Conf. Power Electron. Appl.*, 2014, pp. 1–10.
- [35] Y. Lee, S. Park, and S. Han, "Online embedded impedance measurement using high-power battery charger," *IEEE Trans. Ind. Appl.*, vol. 51, no. 1, pp. 498–508, Jan./Feb. 2015.
- [36] S. K. Dam and V. John, "High-resolution converter for battery impedance spectroscopy," *IEEE Trans. Ind. Appl.*, vol. 54, no. 2, pp. 1502–1512, Mar./Apr. 2018.
- [37] R. Koch and A. Jossen, "Impedance spectroscopy for battery monitoring with switched mode amplifiers," in *Proc. 16th Int. Power Electron. Motion Control Conf. Expo.*, 2014, pp. 496–501.
- [38] S. K. Dam and V. John, "High voltage resolution auxiliary power converter for online battery impedance measurement," in *Proc. IEEE Energy Convers. Congr. Expo.*, 2019, pp. 5450–5457.

- [39] X. Wang, X. Wei, Q. Chen, and H. Dai, "A novel system for measuring alternating current impedance spectra of series-connected Lithium-ion batteries with a high-power dual active bridge converter and distributed sampling units," *IEEE Trans. Ind. Electron.*, early access.
- [40] M. Bayati, M. Abedi, G. B. Gharehpetian, and M. Farahmandrad, "Sinusoidal-ripple current control in battery charger of electric vehicles," *IEEE Trans. Veh. Technol.*, vol. 69, no. 7, pp. 7201–7210, Jul. 2020.
- [41] A. Benshatti, S. M. R. Islam, T. Link, S. Park, and S. Park, "Design and control of AC current injector for battery EIS measurement," in *Proc. IEEE Appl. Power Electron. Conf. Expo.*, 2020, pp. 3452–3455.
- [42] E. Din, C. Schaeff, K. Moffat, and J. T. Stauth, "A scalable active battery management system with embedded real-time electrochemical impedance spectroscopy," *IEEE Trans. Power Electron.*, vol. 32, no. 7, pp. 5688–5698, Jul. 2017.
- [43] T. R. B. Grandjean, J. Groenewald, A. McGordon, W. D. Widanage, and J. Marco, "Accelerated internal resistance measurements of lithium-ion cells to support future End-of-Life strategies for electric vehicles," *Batteries*, vol. 4, 2018, Art. no. 49.
- [44] Z. Gong *et al.*, "EV BMS with distributed switch matrix for active balancing, online electrochemical impedance spectroscopy, and auxiliary power supply," in *Proc. 21st Eur. Conf. Power Electron. Appl.*, 2019, pp. P.1–P.10.
- [45] Z. Gong *et al.*, "IC for online EIS in automotive batteries and hybrid architecture for high-current perturbation in low-impedance cells," in *Proc. IEEE Appl. Power Electron. Conf. Expo.*, 2018, pp. 1922–1929.
- [46] C. Brivio, V. Musolino, M. Merlo, and C. Ballif, "A physically-based electrical model for lithium-ion cells," *IEEE Trans. Energy Convers.*, vol. 34, no. 2, pp. 594–603, Jun. 2019.
- [47] S. Buller, M. Thele, R. W. A. A. De Doncker, and E. Karden, "Impedance-based simulation models of supercapacitors and Li-ion batteries for power electronic applications," *IEEE Trans. Ind. Appl.*, vol. 41, no. 3, pp. 742–747, May/Jun. 2005.
- [48] H. Nara, T. Yokoshima, and T. Osaka, "Technology of electrochemical impedance spectroscopy for an energy-sustainable society," *Curr. Opinion Electrochem.*, vol. 20, pp. 66–77, 2020.
- [49] A. M. Bizeray, J. Kim, S. R. Duncan, and D. A. Howey, "Identifiability and parameter estimation of the single particle lithium-ion battery model," *IEEE Trans. Control Syst. Technol.*, vol. 27, no. 5, pp. 1862–1877, Sep. 2019.
- [50] D. Andre, M. Meiler, K. Steiner, H. Walz, T. Soczka-Guth, and D. U. Sauer, "Characterization of high-power lithium-ion batteries by electrochemical impedance spectroscopy. II: Modelling," *J. Power Sources*, vol. 196, no. 12, pp. 5349–5356, 2011.
- [51] S. Skoog and S. David, "Parameterization of linear equivalent circuit models over wide temperature and SOC spans for automotive lithium-ion cells using electrochemical impedance spectroscopy," *J. Energy Storage*, vol. 14, pp. 39–48, 2017.
- [52] M. Koseoglou, E. Tsioumas, N. Jabbour, and C. Mademlis, "Highly effective cell equalization in a lithium-ion battery management system," *IEEE Trans. Power Electron.*, vol. 35, no. 2, pp. 2088–2099, Feb. 2020.
- [53] A. Lasia, *Electrochemical Impedance Spectroscopy and Its Applications*. Berlin, Germany: Springer, 2014.
- [54] Y. F. Pulido, C. Blanco, D. Anseán, V. M. García, F. Ferrero, and M. Valledor, "Determination of suitable parameters for battery analysis by electrochemical impedance spectroscopy," *Measurement*, vol. 106, pp. 1–11, 2017.
- [55] A. Barai, G. H. Chouchelamane, Y. Guo, A. McGordon, and P. Jennings, "A study on the impact of lithium-ion cell relaxation on electrochemical impedance spectroscopy," *J. Power Sources*, vol. 280, pp. 74–80, 2015.
- [56] L. Deleebeeck and S. Veltzé, "Electrochemical impedance spectroscopy study of commercial Li-ion phosphate batteries: A metrology perspective," *Int. J. Energy Res.*, vol. 44, pp. 7158–7182, 2020.
- [57] N. Meddings *et al.*, "Application of electrochemical impedance spectroscopy to commercial Li-ion cells: A review," *J. Power Sources*, vol. 480, 2020, Art. no. 228742.
- [58] M. Ma, Q. Duan, C. Zhao, Q. Wang, and J. Sun, "Faulty characteristics and identification of increased connecting and internal resistance in parallel-connected Lithium-ion battery pack for electric vehicles," *IEEE Trans. Veh. Technol.*, vol. 69, no. 10, pp. 10797–10808, Oct. 2020.
- [59] Y. Cao and J. AbuQahouq, "Hierarchical SOC balancing controller for battery energy storage system," *IEEE Trans. Ind. Electron.*, early access.



Markos Koseoglou (Student Member, IEEE) was born in Thessaloniki, Greece, on July 11, 1992. He received the Diploma degree in 2018 from the School of Electrical and Computer Engineering, Aristotle University of Thessaloniki, Thessaloniki, Greece, where he is currently working toward the Ph.D. degree in battery management system optimization.

His research interests include energy management in power systems, battery management systems, and embedded systems design.



Evangelos Tsioumas (Student Member, IEEE) was born in Kompotades Fthiotidas, Greece, on June 13, 1988. He received the Diploma degree in 2013 from the School of Electrical and Computer Engineering, Aristotle University of Thessaloniki, Thessaloniki, Greece, where he is currently working toward the Ph.D. degree in energy management optimization in microgrids.

His research interests include energy management in power systems, control optimization in microgrids, large-scale electric energy storage systems, and embedded systems design.



Dimitrios Papagiannis (Student Member, IEEE) was born in Kranea Elassonas, Greece, on December 24, 1990. He received the Diploma degree in 2015 from the School of Electrical and Computer Engineering, Aristotle University of Thessaloniki, Thessaloniki, Greece, where he is currently working toward the Ph.D. degree in optimization of vehicles' active suspension systems.

His research interests include performance improvement of active suspension systems in vehicles, vehicle dynamics, electric motor drives, power electronics, and embedded systems design.



Nikolaos Jabbour was born in Thessaloniki, Greece, on December 4, 1988. He received the Dipl. Eng. and Ph.D. degrees in electrical and computer engineering from the Aristotle University of Thessaloniki, Thessaloniki, Greece, in 2012 and 2018, respectively.

Since 2018, he has been with the Electrical Machines Laboratory, School of Electrical and Computer Engineering, Aristotle University of Thessaloniki, as a Postdoctoral Researcher. His research interests include control optimization, electrical machines and drives, power electronics, embedded systems, renewable energy systems, smart grids, and energy management in nearly zero-energy buildings.



Christos Mademlis (Senior Member, IEEE) was born in Arnea Chalkidikis, Greece, on February 7, 1964. He received the Diploma degree in electrical engineering (first class hons.) and the Ph.D. degree in electrical machines from the Aristotle University of Thessaloniki, Thessaloniki, Greece, in 1987 and 1997, respectively.

Since 1990, he has been with the Electrical Machines Laboratory, Faculty of Electrical and Computer Engineering, Aristotle University of Thessaloniki, as a Research Associate (1990–2001), a Lecturer (2001–2006), an Assistant Professor (2007–2014), an Associate Professor (2014–2019), and is currently a Professor (since 2019). From 2013 to 2016, he was the Head of the Department of Electrical Energy, and since 2010 he has been the Director of the Electrical Machine Laboratory, Faculty of Engineering, Aristotle University of Thessaloniki. He has authored and coauthored more than 75 peer-reviewed technical papers. His research interests include electrical machines and drives, especially in design and control optimization, renewable energy sources, electric vehicles, energy saving systems, and energy management in nearly zero-energy buildings.

Prof. Mademlis was the Founder, in 2013, and the Faculty Advisor, from 2013 to 2017, of the Student Formula SAE Racing Team of the Aristotle University of Thessaloniki. In 2017, he was the recipient of the Fulbright Grant as a Visiting Professor at the APED, Electrical and Computer Engineering Department, University of Connecticut, Storrs, CT, USA.